Formation of On- and Off-Pathway Intermediates in the Folding Kinetics of *Azotobacter vinelandii* Apoflavodoxin†

Yves J. M. Bollen,‡ Ignacio E. Sánchez,§ and Carlo P. M. van Mierlo*,‡

Department of Agrotechnology and Food Sciences, Laboratory of Biochemistry, Wageningen University, Dreijenlaan 3, NL-6703 HA Wageningen, The Netherlands, and Department of Biophysical Chemistry, Biozentrum der Universität Basel, Klingelbergstrasse 70, CH-4056 Basel, Switzerland

Received March 8, 2004; Revised Manuscript Received May 13, 2004

ABSTRACT: The folding kinetics of the 179-residue *Azotobacter vinelandii* apoflavodoxin, which has an $\alpha-\beta$ parallel topology, have been followed by stopped-flow experiments monitored by fluorescence intensity and anisotropy. Single-jump and interrupted refolding experiments show that the refolding kinetics involve four processes yielding native molecules. Interrupted unfolding experiments show that the two slowest folding processes are due to Xaa−Pro peptide bond isomerization in unfolded apoflavodoxin. The denaturant dependence of the folding kinetics is complex. Under strongly unfolding conditions (>2.5 M GuHCl), single exponential kinetics are observed. The slope of the chevron plot changes between 3 and 5 M denaturant, and no additional unfolding process is observed. This reveals the presence of two consecutive transition states on a linear pathway that surround a high-energy on-pathway intermediate. Under refolding conditions, two processes are observed for the folding of apoflavodoxin molecules with native Xaa−Pro peptide bond conformations, which implies the population of an intermediate. The slowest of these two processes becomes faster with increasing denaturant concentration, meaning that an unfolding step is rate-limiting for folding of the majority of apoflavodoxin molecules. It is shown that the intermediate that populates during refolding is off-pathway. The experimental data obtained on apoflavodoxin folding are consistent with the linear folding mechanism $I_{off} \leftrightarrow U \leftrightarrow I_{on} \leftrightarrow N$, the off-pathway intermediate being the molten globule one that also populates during equilibrium denaturation of apoflavodoxin. The presence of such on-pathway and off-pathway intermediates in the folding kinetics of $\alpha-\beta$ parallel proteins is apparently governed by protein topology.

It is still not well understood how an unfolded protein finds its unique native tertiary structure among an astronomically large number of possible conformations. The topology of a protein is proposed to control folding. A strong correlation has been found between topological characteristics and folding rates (*1*). In addition, the structure of the folding transition state can to some extent also be predicted from topology (*2*). However, little is known about whether topology controls the formation of intermediates and the role they play in the kinetic folding mechanism (*3*, *4*).

Various single-domain proteins form an intermediate structure before they fold to their native state (*5*−*8*). Whether folding intermediates are productive forms on the folding route or misfolded off-pathway species has been a subject of discussion for a long time (*9*, *10*). An evaluation of experimental data on 23 proteins that apparently fold in a two-state manner and display nonlinear activation free energy relationships has gained evidence for the involvement of obligatory high-energy on-pathway intermediates in protein folding (*11*). Recent insight suggests that whether an intermediate appears to be on or off the direct folding route depends to some extent on the experimental conditions used. There may be several parallel routes toward the native state, and relatively small changes in the environment or in the sequence of the protein may drastically alter the population of different parallel pathways (*12*−*14*).

The study of the role of intermediates during folding is facilitated when these intermediates populate both kinetically and at equilibrium. Equilibrium population of an intermediate facilitates the determination of its structure, which can clarify why it is on or off the direct folding route under certain circumstances. This population is more likely to happen for large proteins (>100 residues), which therefore offer a special opportunity to study the role of intermediates in protein folding mechanisms.

The relatively large, 179-residue apoflavodoxin from *Azotobacter vinelandii* populates an intermediate with molten globule-like characteristics during denaturant-induced and thermally induced equilibrium denaturation of the protein (*15*, *16*). Flavodoxins are flavoproteins that function as low-potential one-electron carriers and contain a noncovalently bound flavin mononucleotide (FMN)[1] cofactor (*17*). Apoflavodoxin from *A. vinelandii* (i.e., flavodoxin in the absence

† This work is supported by a grant from the NWO−Unilever research programme, Computational Chemistry of Biosystems, and by a grant from the Swiss National Science Foundation.

* Corresponding author. Phone: +31 317 484621. Fax: +31 317 484801. E-mail: carlo.vanmierlo@wur.nl.

‡ Wageningen University.

§ Biozentrum der Universität Basel.

[1] Abbreviations: CD, circular dichroism; FMN, flavin mononucleotide; GuHCl, guanidine hydrochloride.

10.1021/bi049545m CCC: $27.50
Published on Web 07/17/2004

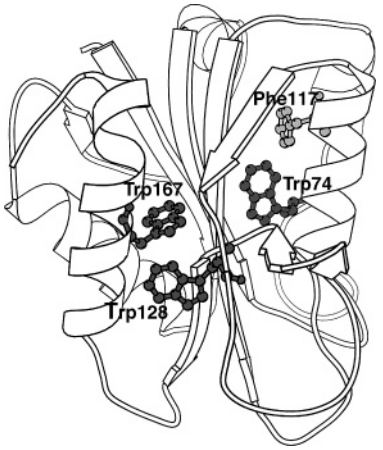

FIGURE 1: MOLSCRIPT cartoon drawing (*45*) of the X-ray structure of *Azotobacter chroococcum* flavodoxin (*46*), the sequence of which is 95% identical to *A. vinelandii* flavodoxin. The side chains of the three tryptophan residues of *A. vinelandii* flavodoxin (dark gray) and of phenylalanine 117 (light gray) are shown in ball-and-stick representation.

of the FMN cofactor) is structurally identical to flavodoxin except for some dynamic disorder in the flavin-binding region (*18*, *19*).

Flavodoxins adopt the so-called doubly wound or $\alpha-\beta$ parallel topology. They are all characterized by a five-stranded parallel β-sheet surrounded by α-helices at either side of the sheet (Figure 1). The doubly wound topology is a rather popular fold: it belongs to the five most common observed folds, together with the TIM barrel, Rossman, thiamin-binding, and P-loop hydrolase folds (*20*). In contrast to most protein folds, this topology is shared by many (i.e., nine) protein superfamilies (*21*). These nine superfamilies exhibit little or no sequence similarity and comprise a broad range of unrelated proteins with different functions such as catalases, chemotactic proteins, lipases, esterases, and flavodoxins.

Here, we present the experimental results of a kinetic folding study of *A. vinelandii* apoflavodoxin and discuss the influence of protein topology on the occurrence of kinetic folding intermediates. It is shown that kinetic folding of apoflavodoxin involves two intermediates. The change in denaturant accessibility upon unfolding of the first intermediate is 29% of that of native apoflavodoxin, and the intermediate has to unfold before formation of the native state can occur. Instead, the second intermediate lies on a direct route from the unfolded to the native state of the protein, and the change in denaturant accessibility upon unfolding of the second intermediate is approximately 80−90% of that of native apoflavodoxin. It is shown that the off-pathway intermediate is the one that populates during equilibrium denaturation of apoflavodoxin. The kinetic results presented on apoflavodoxin folding lead to the first experimental identification of both intermediates predicted theoretically to exist during the folding of an $\alpha-\beta$ parallel protein (*22*).

MATERIALS AND METHODS

Materials. Guanidine hydrochloride (GuHCl, ultrapure) and potassium pyrophosphate were from Sigma (Bornem, Belgium).

Protein Expression and Purification. The single cysteine residue 69 in wild-type *A. vinelandii* (strain ATCC 478) flavodoxin II was replaced by an alanine to avoid covalent dimerization of apoflavodoxin. The mutant protein is largely similar to wild-type flavodoxin regarding both redox potential of the holoprotein and stability of the apoprotein (*15*, *23*). Recombinant *A. vinelandii* C69A holoflavodoxin was obtained and purified as described previously (*15*, *18*). Apoflavodoxin was subsequently prepared by trichloroacetic acid preparation (*15*, *24*). Finally, apoflavodoxin molecules in an oligomeric state were removed via gel filtration on a Superdex 200 preparative grade column (Pharmacia, Uppsala, Sweden).

Fluorescence Spectroscopy. Steady-state fluorescence measurements were done on a Cary eclipse fluorometer equipped with a peltier accessory (Varian, Palo Alto, CA). Excitation was at 280 nm with a slit of 5 nm; emission spectra were recorded from 320 to 360 nm in steps of 0.5 nm, using a slit of 2.5 nm. The temperature was 25 °C in all experiments; the protein concentration was 5.6 μM in 100 mM potassium pyrophosphate, pH 6.0. All samples were equilibrated overnight at 25 °C.

Circular Dichroism (CD) Spectroscopy. Steady-state CD measurements were performed on a Jasco J715 spectropolarimeter (Tokyo, Japan) equipped with a PTC-348WI peltier temperature control system. GuHCl denaturation samples were measured in a 1 mm quartz cuvette (Starna, Hainault, England) at 222, 225, and 255 nm and averaged over 3 min per wavelength at a temperature of 25 °C. The ellipticity at 255 nm was subtracted from the other ellipticities as a baseline value. During all experiments the cell chamber was purged with dry nitrogen gas at a flow rate of 5 L/min. All samples were equilibrated overnight at 25 °C; the protein concentration was 5.6 μM in 100 mM potassium pyrophosphate, pH 6.0.

Fluorescence Anisotropy. Fluorescence anisotropy was measured on a home-built fluorometer equipped with two photomultipliers arranged in a T-format (Thorn EMI 9863QA/350, operating in photon-counting detection mode). Excitation light was generated by a 150 W short arc xenon lamp, and the excitation wavelength of 300 nm was selected in a monochromator (Bausch & Lomb, Rochester, NY) with a band-pass of 4.8 nm. Polarizers were used in both the excitation light path (rotable Glan Taylor polariser) and the emission light path (Polaroid, sheet). The emission light was selected with a 335 nm cutoff filter (Schott). A blank measurement, containing all components except apoflavodoxin, was subtracted from each sample, and five measurements were averaged for each sample. The measurement chamber was thermostated at 25 °C by a circulating water bath. All samples were equilibrated overnight at 25 °C; the protein concentration was 5.6 μM in 100 mM potassium pyrophosphate, pH 6.0.

Stopped-Flow Fluorescence Spectroscopy. Stopped-flow folding and unfolding experiments were performed on an Applied Photophysics (Leatherhead, U.K.) SX18-MV instrument with a 5 or 20 μL cell. The path length of the observation chamber was 2 mm. Excitation was at 280 nm with a slit of 1.85 nm, and a cutoff filter of 320 nm was used to select the emitted light. In unfolding experiments apoflavodoxin in 100 mM potassium pyrophosphate, pH 6.0, was mixed 1:10 into the same buffer containing varying

concentrations of GuHCl. In refolding experiments apoflavodoxin was first unfolded in 5.0 M GuHCl in 100 mM potassium pyrophosphate, pH 6.0, for at least 30 min and subsequently diluted 1:10 or 1:25 into the same buffer with a varying concentration of GuHCl. The final concentration of apoflavodoxin in the observation cell was 1 μM in all cases. At least four curves were averaged for each final denaturant concentration. The syringes and observation chamber were thermostated at 25 °C by a circulation water bath.

(a) Refolding Kinetics of Freshly Unfolded Apoflavodoxin. The influence of the presence of *cis*-proline isomers on the faster folding rates was examined by refolding freshly unfolded protein. The same experimental setup as described for the stopped-flow measurements was used but now in the sequential mixing mode.

Apoflavodoxin was first unfolded at 3 M GuHCl in 100 mM potassium pyrophosphate, pH 6.0, by a 1:6 mixing step. After 622 ms, refolding was initiated by 1:6 mixing into the same buffer containing various concentrations of GuHCl. The final protein concentration in the observation chamber was always 1 μM. At least four curves were averaged for each final denaturant concentration.

(b) Interrupted Unfolding of Apoflavodoxin. Interrupted unfolding was used to examine the origin of the different refolding processes. Apoflavodoxin was first unfolded at 3 M GuHCl for a varying time t_i and then refolded by 1:6 mixing into native buffer, to yield a final GuHCl concentration of 0.5 M and a final protein concentration of 1 μM in 100 mM potassium pyrophosphate, pH 6.0. At least four curves were averaged for each t_i. The t_i-dependent amplitude of each individual refolding process gives the rate with which the species causing the respective refolding process is formed during the unfolding step at 3 M GuHCl.

Analogously, interrupted unfolding by manual mixing was used to examine the origin of the slowest folding process. A volume of 0.4 mL of a 30 μM apoflavodoxin stock solution was mixed into 0.6 mL of a 5 M GuHCl solution. After a varying time t_i, 0.4 mL of this solution was mixed into a 3 mL fluorescence cuvette containing 2 mL of stirred buffer to result in a final protein concentration of 2 μM and a final GuHCl concentration of 0.5 M in 100 mM potassium pyrophosphate, pH 6.0. Refolding traces of 100 s were recorded. All solutions were preequilibrated at 25 °C. Fluorescence traces were recorded on a Varian Cary Eclipse fluorometer using an excitation wavelength of 280 nm, an excitation slit of 5 nm, and an emission wavelength of 330 nm with a 20 nm slit.

(c) Interrupted Refolding of Apoflavodoxin. Interrupted refolding was used to examine whether all rates observed in refolding lead to native protein. Unfolded apoflavodoxin at 5 M GuHCl was first allowed to refold at 0.83 M GuHCl for a varying time t_i and subsequently unfolded at 5 M GuHCl. The buffer used was 100 mM potassium pyrophosphate, pH 6.0. The amplitude corresponding to the observed unfolding process was used as a measure for the formation of native apoflavodoxin during the refolding time t_i. At least four curves were averaged for each t_i.

Stopped-Flow Fluorescence Anisotropy. Stopped-flow fluorescence anisotropy measurements were done on a BioLogic (Claix, France) SFM4 equipped with a 2 × 2 mm cuvette (FC-20), with the additional use of a photoelastic modulator (*25*, *26*). Excitation was at 297 nm with a slit of 1 mm, resulting in a band-pass of 8 nm. A cutoff filter of 335 nm (335FG01-25; Andover Corp.) was used to select the emission light. The solutions in the syringes as well as in the observation chamber were thermostated at 25 °C by a circulating water bath. In the refolding experiment 10 μM apoflavodoxin at 5 M GuHCl in 100 mM potassium pyrophosphate, pH 6.0, was diluted 10-fold into the same buffer without GuHCl, resulting in a final protein concentration of 1 μM at 0.5 M GuHCl. The dead time was 14.8 ms, and 14 curves were averaged. In the unfolding experiment 10 μM apoflavodoxin in 100 mM potassium pyrophosphate, pH 6.0, was diluted 10-fold into the same buffer containing 5 M GuHCl, which results in a final protein concentration of 1 μM and a GuHCl concentration of 4.5 M. Twenty-five curves were averaged.

Data Analysis. (a) Equilibrium Denaturation Data. Apoflavodoxin equilibrium denaturation data as monitored by fluorescence emission intensity (at 340, 350, and 360 nm), circular dichroism (at 222 and 225 nm), and fluorescence anisotropy were globally fitted to a three-state model for equilibrium denaturation (eq 1), according to eqs 2−6, using ProFit (Quantum Soft, Zürich):

$$\mathrm{U} \rightleftarrows \mathrm{I} \rightleftarrows \mathrm{N} \tag{1}$$

$$K_{\mathrm{UI}} = [\mathrm{I}]/[\mathrm{U}], \qquad K_{\mathrm{IN}} = [\mathrm{N}]/[\mathrm{I}] \tag{2}$$

$$K_{ij}(\mathrm{D}) = K_{ij}^{0} \exp(m_{ij}^{\mathrm{eq}}[\mathrm{D}]) \tag{3}$$

$$\begin{aligned} f_{\mathrm{U}} &= 1/(1 + K_{\mathrm{UI}} + K_{\mathrm{UI}}K_{\mathrm{IN}}) \\ f_{\mathrm{I}} &= K_{\mathrm{UI}}/(1 + K_{\mathrm{UI}} + K_{\mathrm{UI}}K_{\mathrm{IN}}) \\ f_{\mathrm{N}} &= K_{\mathrm{UI}}K_{\mathrm{IN}}/(1 + K_{\mathrm{UI}} + K_{\mathrm{UI}}K_{\mathrm{IN}}) \end{aligned} \tag{4}$$

$$Y^{\mathrm{obs}} = (a_{\mathrm{N}} + b_{\mathrm{N}}[\mathrm{D}])f_{\mathrm{N}} + (a_{\mathrm{I}} + b_{\mathrm{I}}[\mathrm{D}])f_{\mathrm{I}} + (a_{\mathrm{U}} + b_{\mathrm{U}}[\mathrm{D}])f_{\mathrm{U}} \tag{5}$$

U, I, and N represent the unfolded, intermediate, and native state of the protein, respectively, K_{ij} is the equilibrium constant of the $i-j$ equilibrium, K_{ij}^{0} is the $i-j$ equilibrium constant at zero concentration denaturant, [D] is the denaturant concentration, m_{ij}^{eq} is the constant that describes the denaturant concentration dependence of the equilibrium constant K_{ij}, f_i is the fractional population of state i at a certain denaturant concentration, Y^{obs} is the observed spectroscopic signal, a_i is the spectroscopic property of state i at zero concentration denaturant, and b_i is the constant describing the denaturant concentration dependence of the spectroscopic signal of state i. Each individual data point was weighted by the square of the corresponding standard error during the global fit procedure.

To incorporate the fluorescence anisotropy data in the global analysis procedure, a modification of eq 5 is required. Unlike fluorescence emission intensity and circular dichroism signals, fluorescence anisotropy signals do not linearly track the mole fractions of the three states of apoflavodoxin. This is due to the anisotropy signals being weighted by both the fraction of states involved and by the fluorescence quantum yield of each individual state (*27*). To describe the anisotropy signal adequately, the fraction of each species was multiplied

with its intrinsic anisotropy (with corresponding denaturant concentration dependence) and weighted by its fluorescence intensity at 360 nm, according to the equation:

$$Y^{obs}_{anisotropy} = [(a_{N,Fl} + b_{N,Fl}[D])(a_{N,anis} + b_{N,anis}[D])f_N + (a_{I,Fl} + b_{I,Fl}[D])(a_{I,anis} + b_{I,anis}[D])f_I + (a_{U,Fl} + b_{U,Fl}[D])(a_{U,anis} + b_{U,anis}[D])f_U]/[(a_{N,Fl} + b_{N,Fl}[D]) + (a_{I,Fl} + b_{I,Fl}[D]) + (a_{U,Fl} + b_{U,Fl}[D])] \quad (6)$$

with $a_{i,Fl}$ being the intrinsic fluorescence intensity of species i at 360 nm, $b_{i,Fl}$ the denaturant concentration dependence of $a_{i,Fl}$, and $a_{i,anis}$ and $b_{i,anis}$ the intrinsic anisotropy of state i and its corresponding denaturant concentration dependence, respectively.

The fluorescence emission spectrum of the equilibrium intermediate was calculated by fitting the equilibrium denaturation curves at all fluorescence emission wavelengths measured (320−360 nm) to eqs 2−5 with the equilibrium constants K_{UI} and K_{IN} fixed to the values determined in the global fit mentioned before, using the program MatLab (Mathworks).

(b) Kinetic (Un)folding Data. All kinetic fluorescence data and the t_i-dependent refolding and unfolding amplitudes in double-jump experiments were fitted to sums of exponential functions using ProFit (Quantum Soft, Zürich).

Of the four observed rate constants in stopped-flow (un)-folding experiments, rate constant λ_2 was fitted to the four-state linear folding mechanism described in Scheme 1.

Scheme 1

$$I_1 \underset{k_{UI_1}}{\overset{k_{I_1U}}{\rightleftharpoons}} U \underset{k_{I_2U}}{\overset{k_{UI_2}}{\rightleftharpoons}} I_2 \underset{k_{NI_2}}{\overset{k_{I_2N}}{\rightleftharpoons}} N$$

In this linear scheme, U corresponds to unfolded protein, N corresponds to native protein, I_1 and I_2 correspond to the off-pathway and on-pathway folding intermediate, respectively, and k_{ij} corresponds to the microscopic rate constant from state i to state j. Use is made of the analytical solution of a four-state folding mechanism as described by Ikai and Tanford (*28*), and an exponential dependence of the microscopic rate constants on the denaturant concentration is assumed, as described by the equation:

$$k_{ij} = k^0_{ij} \exp(m_{ij}[D]) \quad (7)$$

with k_{ij} being the intrinsic rate constant for the transition from state i to j at a certain denaturant concentration [D], k^0_{ij} the rate constant k_{ij} at zero concentration denaturant, and m_{ij} the constant that describes the denaturant concentration dependence of k_{ij}. The rate constant k_{I_2N} and the corresponding m_{I_2N} were fixed to 10^5 and 0, respectively (see Results and Discussion for explanation).

RESULTS AND DISCUSSION

Equilibrium Denaturation of A. vinelandii Apoflavodoxin Involves a Populated Intermediate. The equilibrium denaturation of *A. vinelandii* apoflavodoxin with GuHCl is followed by both circular dichroism (CD) and fluorescence emission spectroscopy. In Figure 2A the fractions of native apoflavodoxin molecules are shown, based on the fluorescence emission data at 340 nm and the ellipticity values at 222 nm, each analyzed according to a two-state model (*29*) for denaturation. The fit of the fluorescence data results in a global apoflavodoxin stability of 6.24 ± 0.25 kcal/mol, with a corresponding m-value of −4.07 ± 0.16 kcal mol^{-1} M^{-1}, resulting in a GuHCl concentration at the midpoint of denaturation (C_m) of 1.533 ± 0.007 M. The fit of the CD data results in a global apoflavodoxin stability of 2.91 ± 0.30 kcal/mol, with a corresponding m-value of −1.69 ± 0.14 kcal mol^{-1} M^{-1}, resulting in a C_m of 1.72 ± 0.05 M GuHCl, values that are all significantly different from those determined on the basis of the fluorescence data. The denaturation curves obtained by CD and fluorescence spectroscopy do not coincide, which is characteristic for the population of an intermediate in equilibrium apoflavodoxin denaturation, as reported previously (*15*). Analogously, thermal denaturation of apoflavodoxin results in apparent midpoint temperatures of 48.6 ± 0.1 °C (fluorescence) and 64.9 ± 0.4 °C (CD), a difference of 16.3 °C (*15*).

The anisotropy of tryptophan fluorescence can also be used to monitor the equilibrium denaturation transition of a protein and often gives quite different results compared to fluorescence intensity measurements (*26*, *30*, *31*). The apoflavodoxin denaturation curve measured by anisotropy shown in Figure 2B is clearly biphasic, which illustrates the need of a folding intermediate to describe the equilibrium denaturation data of apoflavodoxin.

A three-state model (eqs 1−6) is fitted globally to all apoflavodoxin equilibrium denaturation curves recorded, i.e., at two CD wavelengths (222 and 225 nm) and at three fluorescence intensity wavelengths (340, 350, and 360 nm) and obtained by fluorescence anisotropy. The denaturant dependence of the spectroscopic parameters of the intermediate (b_I in eq 5) cannot be accurately determined because the intermediate populates only in a small range of GuHCl concentrations and never populates for 100%. Therefore, b_I is set to zero in the global fit procedure. The global fit of the three-state model to all apoflavodoxin denaturation data is excellent (see, e.g., Figure 2B,C), and the results are summarized in Table 1. In Figure 2C the results of the global fit to the equilibrium denaturation data of apoflavodoxin as observed by CD at 222 nm and fluorescence intensity at 340 nm are shown (the same data as used to construct the curves in Figure 2A are again used). As can be judged from the residuals (Figure 2D) the equilibrium data shown in Figure 2C are well described by a three-state fit. In conclusion, at least one intermediate state populates in the transition zone of denaturant-induced apoflavodoxin denaturation.

The stabilities against global unfolding of both native apoflavodoxin and of its equilibrium folding intermediate as presented in Table 1 are higher than those reported previously (*15*). This is mainly caused by differences in the assumptions made about the spectroscopic properties of the apoflavodoxin equilibrium folding intermediate. In the previous analysis (*15*), the fluorescence intensity of the intermediate is assumed to be equal to the one of the unfolded state, and the CD ellipticity of the intermediate is set equal to the one of native apoflavodoxin. Due to the limited number of data points, the original data of van Mierlo et al. (*15*) do not allow the sophisticated analysis presented here in which fluorescence intensities and CD ellipticities of the equilibrium folding intermediate are treated as free parameters.

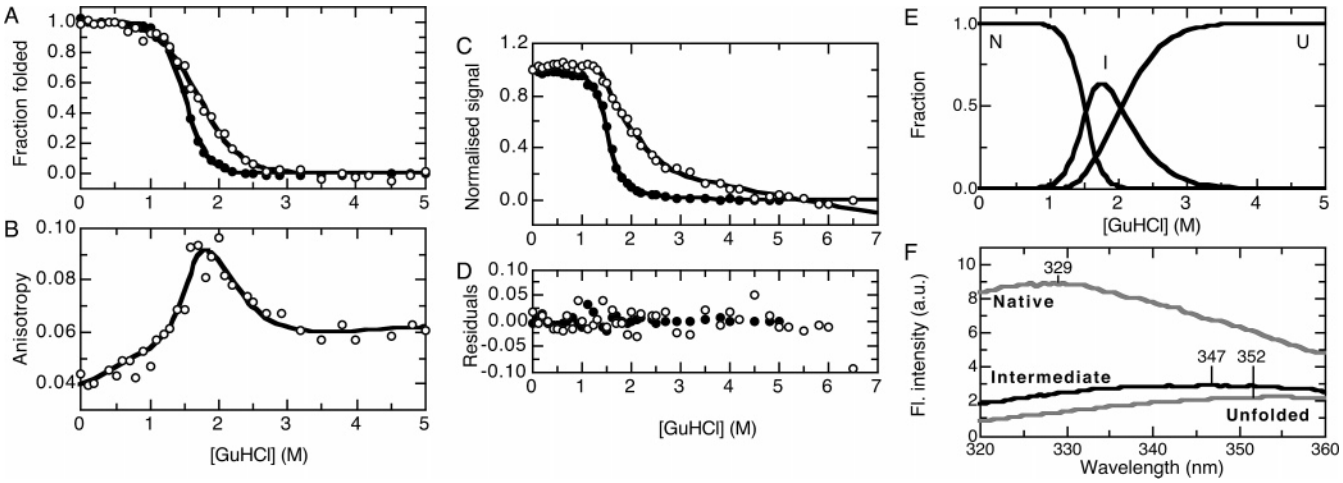

FIGURE 2: Guanidine hydrochloride-induced equilibrium denaturation of *A. vinelandii* apoflavodoxin. The protein concentration is 5.6 μM in 100 mM potassium pyrophosphate, pH 6.0, and the data are recorded at 25 °C. (A) The fluorescence emission intensity data recorded at 340 nm (●) and the circular dichroism data recorded at 222 nm (○) are each separately analyzed according to a two-state model for folding, and the resulting fractions of native apoflavodoxin molecules are shown. The curves do not coincide, as a folding intermediate populates during apoflavodoxin denaturation. (B) Guanidine hydrochloride denaturation profile of apoflavodoxin as measured by fluorescence anisotropy. The curve is clearly biphasic, due to the population of an intermediate during apoflavodoxin denaturation. (C) The fluorescence and CD data of apoflavodoxin denaturation at 340 and 222 nm, respectively, are normalized such that the first data point has a value of 1 and the last data point has a value of 0 (the same data as used to construct the curves in panel A are again used). The solid lines in panels B and C represent the result of a global fit of a three-state model for equilibrium denaturation to the fluorescence data at 340, 350, and 360 nm, to the CD data at 222 and 225 nm, and to the anisotropy data in panel B, according to eqs 1−6 (see Materials and Methods). (D) Residuals of the global fit of a three-state model for apoflavodoxin equilibrium denaturation to the fluorescence data at 340 nm (●) and the CD data at 222 nm (○) shown in panel C. (E) Normalized population of native (N), intermediate (I), and unfolded (U) apoflavodoxin molecules as a function of the concentration GuHCl. (F) Computed fluorescence emission spectrum of the equilibrium folding intermediate of apoflavodoxin at 1.6 M GuHCl based on the global fit of a three-state model (eq 1) to the equilibrium denaturation data of *A. vinelandii* apoflavodoxin. The fluorescence emission spectra of native apoflavodoxin and of unfolded apoflavodoxin, both at 1.6 M GuHCl, are shown in gray. The fluorescence emission maxima are shown for all three species. The thermodynamic parameters resulting from the three-state fit to the apoflavodoxin denaturation data are summarized in Table 1.

Table 1: Thermodynamic Parameters Obtained from a Three-State Fit (N ⇔ I ⇔ U) to the GuHCl-Induced Equilibrium Denaturation Data of *A. vinelandii* Apoflavodoxin[a]

ΔG_{UI} (kcal/mol)	3.74 ± 0.49	m_{UI}^{eq} (kcal mol^{-1} M^{-1})	-1.83 ± 0.19
ΔG_{IN} (kcal/mol)	6.70 ± 0.17	m_{IN}^{eq} (kcal mol^{-1} M^{-1})	-4.40 ± 0.11
ΔG_{UN} (kcal/mol)	10.45 ± 0.52	m_{UN}^{eq} (kcal mol^{-1} M^{-1})	-6.23 ± 0.23

[a] A three-state model of unfolding is globally fitted according to eqs 1−6 to the GuHCl-induced equilibrium denaturation curves of *A. vinelandii* apoflavodoxin as obtained by CD at 222 and 225 nm, by fluorescence intensity at 340, 350, and 360 nm, and by fluorescence anisotropy. The errors shown are standard deviations. U, I, and N represent the unfolded, intermediate, and native state of apoflavodoxin. ΔG_{XY} is the difference in free energy between species *X* and *Y* at 0 M denaturant, and m_{XY}^{eq} is the dependence of ΔG_{XY} on the denaturant concentration.

To investigate whether the ionic nature of GuHCl causes the observed population of an apoflavodoxin intermediate, the equilibrium denaturation of apoflavodoxin has also been measured using urea as the denaturant and fluorescence intensity and CD as spectroscopic probes. The obtained urea-induced denaturation curves are similar to the ones presented here (data not shown). As the urea-induced equilibrium denaturation curves of apoflavodoxin measured by fluorescence and CD also do not coincide, it is ruled out that the apoflavodoxin folding intermediate is observed due to a stabilization caused by the salt effect of GuHCl.

Spectroscopic Properties of the Intermediate Observed during Equilibrium Denaturation of A. vinelandii Apoflavodoxin. In this section a low-resolution structural description of the equilibrium folding intermediate of apoflavodoxin is constructed on the basis of the available spectroscopic data.

The fitted denaturant concentration dependencies of the stability of both native apoflavodoxin and of its equilibrium folding intermediate, together with the recorded fluorescence emission spectra between 320 and 360 nm at all GuHCl concentrations used, enable the calculation of the fluorescence emission spectrum of the equilibrium intermediate (Figure 2F). Despite the emission spectrum of the intermediate being quite similar to the emission spectrum of unfolded apoflavodoxin, which is shown in Figure 2F as a reference, they are not identical. The limited blue shift of the fluorescence emission maximum (5 nm) and increased fluorescence intensity of the intermediate relative to unfolded apoflavodoxin indicate that the tryptophan residues experience on average some shielding from the solvent. The change in denaturant accessibility upon unfolding of the equilibrium intermediate can be calculated from the reported equilibrium denaturation *m*-values (*32*) in Table 1 and is 29% of that of the native protein.

The difference in ellipticity between the intermediate and the unfolded state of apoflavodoxin at 0 M GuHCl is 65% of the corresponding ellipticity difference between native and unfolded apoflavodoxin at both 222 and 225 nm. Consequently, approximately 65% of the native α-helical content of apoflavodoxin is probably present in the equilibrium intermediate, as at these wavelengths the CD spectrum is especially sensitive to α-helical structure.

Notably, the anisotropy of the apoflavodoxin folding intermediate (Figure 2B), which populates significantly between 1 and 3 M GuHCl, is much higher than the

anisotropy of the native state. Fluorescence anisotropy informs about the rotational freedom of the fluorophore involved. Tryptophan side chains that can rotate freely, as in an unfolded protein, have an anisotropy value of approximately 0.06, depending on the wavelength of excitation and emission. The anisotropy of an immobilized tryptophan side chain in a folded protein depends on the size of the protein. In the case of apoflavodoxin, an anisotropy of 0.10−0.12 is expected when all of its three tryptophan side chains are immobilized (*26*, *30*, *31*).

The observed fluorescence anisotropy of native apoflavodoxin is surprisingly low (i.e., 0.04; Figure 2B). In the case of apoflavodoxin, no indications for a high tryptophan side chain mobility in the native state are observed, since the hydrogen exchange rates of the tryptophan side chain amides of apoflavodoxin correspond to local stabilities of 5−7 kcal/mol (*19*). Apparently, a specific tertiary interaction involving one or more tryptophans causes the low anisotropy of native apoflavodoxin.

The fluorescence of *A. vinelandii* apoflavodoxin arises from its three tryptophan side chains, which are shown in Figure 1. Trp 74 is located in α-helix 3 and is 3.3 Å away from the side chain of Phe 117 in α-helix 4 of apoflavodoxin. The orientation of these aromatic rings relative to one another is close to perpendicular. The fluorescence of Trp 74 is probably quenched by the close-to-perpendicular phenyl ring, as observed in a similar situation for the protein FKBP59-I (*33*). Consequently, the emission spectrum is probably dominated by the two remaining tryptophans. The distance between Trp 128, which is close to β-strand 5a, and Trp 167, which is in helix 5, is 4.5 Å, and their relative orientation in apoflavodoxin is close to perpendicular as well. The two indole rings are well within the Förster distance for resonance energy transfer (RET) of one another (10−15 Å for tryptophans in a hydrophobic protein environment). RET between two tryptophans reduces the fluorescence anisotropy (*34*). Since the two indole rings are in close proximity and almost perpendicular to each other, this reduction in anisotropy would be efficient, explaining the low anisotropy observed for native apoflavodoxin. As a consequence, the equilibrium folding intermediate, as well as other compact structures formed during the folding of apoflavodoxin, is expected to have a higher anisotropy than both native and unfolded apoflavodoxin. In such intermediates the tryptophan side chains can be immobilized, but the highly specific native tertiary interactions that cause the low native anisotropy are not likely. This feature explains the remarkable denaturation profile of apoflavodoxin as observed by fluorescence anisotropy (Figure 2B).

In summary, the apoflavodoxin equilibrium folding intermediate has a fluorescence emission spectrum which shows that its tryptophan side chains are little shielded from the solvent. As can be inferred from fluorescence anisotropy data, these tryptophan side chains are immobilized, but their immediate environment is not fully native. On the basis of CD data, approximately 65% of the α-helical content of native apoflavodoxin is present in the intermediate. The NMR cross-peaks of the equilibrium folding intermediate of apoflavodoxin are extremely broadened, which suggests that this intermediate is highly dynamic on a millisecond to second time scale (*16*). All spectroscopic data put together show that the apoflavodoxin equilibrium folding intermediate has molten globule-like structural characteristics (*35*).

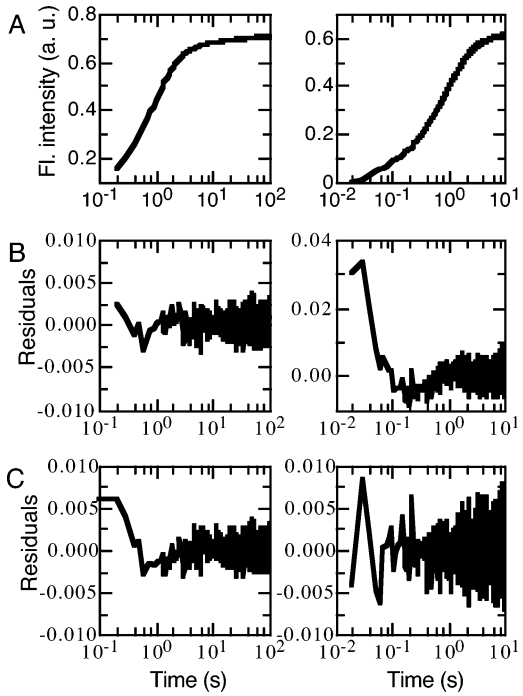

FIGURE 3: Stopped-flow refolding kinetics of *A. vinelandii* apoflavodoxin at 0.56 M GuHCl as observed by tryptophan fluorescence emission intensity. (A) Fluorescence data recorded for a period of 100 s (left) and 10 s (right). Residuals of a fit of a sum of three exponential equations to both data traces are shown in (B). In (C), the residuals of a global fit of a sum of four exponential functions to both the 100 and 10 s data are shown, with $\lambda_1 = 23.6 \pm 1.6$ s^{-1}, $\lambda_2 = 1.16 \pm 0.01$ s^{-1}, $\lambda_3 = 0.33 \pm 0.01$ s^{-1}, and $\lambda_4 = 0.025 \pm 0.001$ s^{-1}. The data are plotted on a logarithmic time scale. The final protein concentration is 1 μM in 100 mM potassium pyrophosphate, pH 6.0, at 25 °C.

Kinetic Characterization of A. vinelandii Apoflavodoxin Folding by Stopped-Flow Fluorescence Shows the Presence of an On-Pathway and an Off-Pathway Intermediate. (a) Refolding Kinetics of Apoflavodoxin Monitored by Intrinsic Trp Fluorescence. To investigate the role of the molten globule-like equilibrium intermediate in the kinetic folding of apoflavodoxin, a stopped-flow folding experiment was performed in 100 mM potassium pyrophosphate, pH 6.0, at 0.56 M GuHCl. Figure 3A shows the refolding of apoflavodoxin recorded by fluorescence spectroscopy for a period of 100 and 10 s, respectively. The fluorescence emission increases with time, because unfolded apoflavodoxin has a lower emission than native protein (Figure 2F). Figure 3B shows the residuals of a fit of a sum of three exponentials to the data. Three exponentials suffice to describe the observed signal in the 100 s trace. However, the 10 s trace is not properly fitted with these three exponentials, which indicates that an additional process is present. As a consequence, a sum of four exponential curves is globally fitted to both 10 and 100 s folding traces. The corresponding residuals of both curves at 0.56 M GuHCl (Figure 3C) show that the data are now correctly described by four folding processes (with folding rate constants λ_1 to λ_4).

(b) Formation of Native Molecules during Apoflavodoxin Folding. To determine whether all four observed processes produce native apoflavodoxin or whether some of the observed processes represent the formation of partially folded

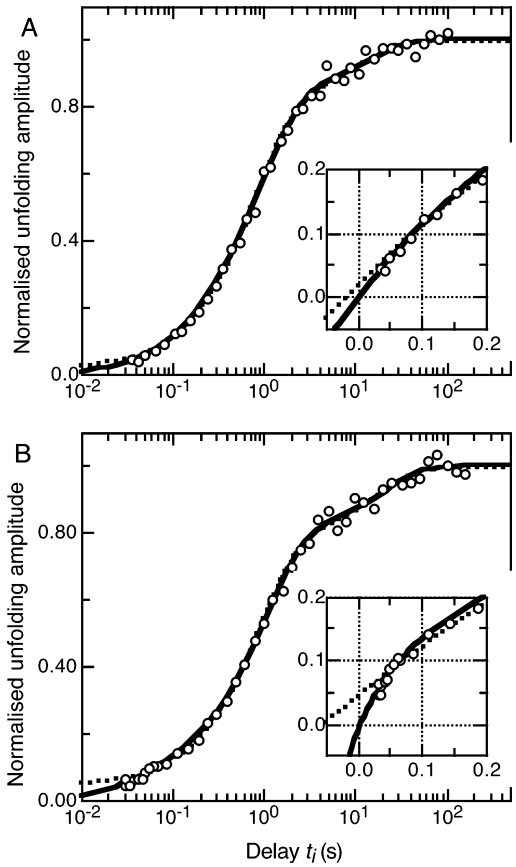

FIGURE 4: Formation of native molecules during refolding of *A. vinelandii* apoflavodoxin. The normalized amplitude of the unfolding process of apoflavodoxin in an interrupted refolding experiment at 0.83 M GuHCl (A) and at 0.42 M GuHCl (B) is shown as a function of the refolding delay time t_i. All data are shown on a logarithmic time scale except in the insets, in which the data obtained during the first 0.2 s of interrupted refolding are shown on a linear time scale. The dashed line is the result of a fit of a sum of two exponentials to the data, and the solid line is the result of a fit of a sum of three exponentials to the data. The inset shows that the data are best described by three exponentials and that in this fit the amplitude of the unfolding process is 0 at $t_i = 0$, as required. The rate constants and corresponding amplitudes are listed in Table 2. The final protein concentration is 1 μM in 100 mM potassium pyrophosphate, pH 6.0, at 25 °C. For further details, see the Materials and Methods section.

intermediates, an interrupted refolding experiment (*12*) was done. In such an experiment, unfolded apoflavodoxin is allowed to fold for a certain time t_i and is subsequently unfolded in 5 M GuHCl and followed by fluorescence spectroscopy. The observed amplitude of the unfolding process, with a rate constant of 48 s^{-1} in the case of *A. vinelandii* apoflavodoxin, is then used as a measure for the amount of native apoflavodoxin that is formed during the refolding time t_i. Generally, folding intermediates unfold much faster than native proteins (*29*), and thus the apoflavodoxin folding intermediates formed during t_i are assumed not to contribute to the observed kinetic trace.

Figure 4 shows the amplitudes of the unfolding processes as a function of the delay time t_i at two different GuHCl concentrations. A fit of a sum of two exponential equations to these data extrapolates to 1.8 ± 0.6% and 4.4 ± 0.4% of all molecules being native at $t_i = 0$, respectively, which would mean that an additional route to the native state is not accounted for in the fit. The data are best described by three exponentials, including a fast process. This fit extrapolates, within experimental error, to 0% of all molecules being native at $t_i = 0$. The two fastest rate constants of the latter fit correspond to the folding rates λ_1 and λ_2 observed during conventional apoflavodoxin refolding at the respective GuHCl concentrations. This shows that native apoflavodoxin is formed in the two fastest processes observed. The third rate constant observed in the interrupted refolding experiment is between λ_3 and λ_4 observed in the conventional refolding experiment. The low sensitivity of the interrupted refolding experiment compared to the direct refolding traces prevents discrimination of the latter two slow processes. The interrupted refolding data at both GuHCl concentrations can be described well using the four respective rate constants observed in direct refolding of apoflavodoxin (Table 2). We interpret this to imply that indeed native apoflavodoxin is formed in all four processes observed in the conventional refolding experiment.

Table 2: Rate Constants (λ_1 to λ_4, in s^{-1}) and Corresponding Amplitudes (A_1 to A_4, in %) Obtained for Direct and Interrupted Refolding of *A. vinelandii* Apoflavodoxin at 0.42 and 0.83 M GuHCl[a]

	0.42 M GuHCl		0.83 M GuHCl	
	direct refolding	interrupted refolding	direct refolding	interrupted refolding
λ_1	12 ± 1	22 ± 3	9.5 ± 1.6	5.6 ± 1.1
A_1	5.9 ± 0.3	8.4 ± 0.3	3.2 ± 0.3	9.1 ± 1.5
λ_2	1.06 ± 0.01	0.97 ± 0.01	1.22 ± 0.01	1.04 ± 0.03
A_2	76 ± 1	71.0 ± 0.6	74.2 ± 0.5	73.8 ± 1.4
λ_3	0.32 ± 0.01		0.29 ± 0.01	
A_3	13.6 ± 0.6		15.0 ± 0.3	
λ_{3-4}		0.048 ± 0.001		0.076 ± 0.004
A_{3-4}		20.6 ± 0.3		17.4 ± 0.5
λ_4	0.021 ± 0.001		0.034 ± 0.001	
A_4	4.24 ± 0.07		7.4 ± 0.1	

[a] For further details, see Materials and Methods. In the case of the interrupted refolding experiments, three exponentials describe the time−course of the data, with the third rate constant (λ_{3-4} with amplitude A_{3-4}) being between rate constants λ_3 and λ_4 observed in the conventional apoflavodoxin kinetic folding experiments. The errors shown are standard deviations. Refolding conditions are 1 μM apoflavodoxin in 100 mM potassium pyrophosphate, pH 6.0, at 25 °C.

(c) Origin of the Parallel Apoflavodoxin Folding Routes. The most common origin of parallel folding routes in proteins is heterogeneity in the unfolded state caused by isomerization around Xaa−Pro peptide bonds (*29*, *36*) or Xaa−non-Pro peptide bonds (*37*). Proline peptide bond isomerization is likely to play a role in *A. vinelandii* flavodoxin folding, because it contains five proline residues. All of the Xaa−Pro peptide bonds are in the trans conformation in the native structure. The percentage of cis peptide bonds of a certain proline residue in equilibrium-unfolded protein depends mainly on the preceding amino acid (*38*). In the case of apoflavodoxin, based on its amino acid sequence, 33% of the molecules are predicted to have at least one *cis*-proline peptide bond in the equilibrium-unfolded state.

To investigate the origin of the parallel folding routes during apoflavodoxin folding, an interrupted unfolding experiment has been performed. Native apoflavodoxin is first unfolded in 3 M GuHCl for a varying delay time t_i and subsequently refolded at 0.5 M GuHCl and followed by fluorescence spectroscopy. The dependence of the amplitudes of the four observed refolding processes (with rate constants

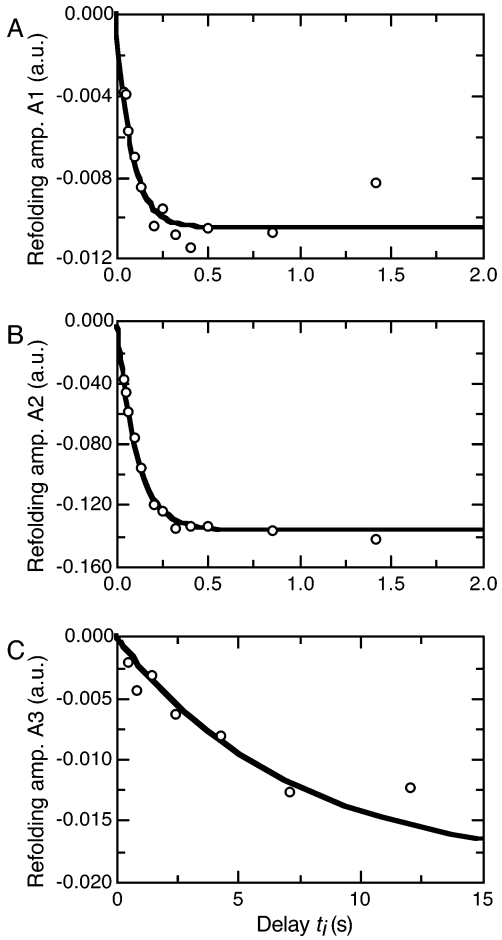

FIGURE 5: Dependence of the amplitudes associated with *A. vinelandii* apoflavodoxin folding rate constants λ_1 to λ_3 on the unfolding time t_i in an interrupted unfolding experiment. In this experiment, native apoflavodoxin is first unfolded in 3 M GuHCl for a varying time t_i, and the subsequent refolding at 0.5 M GuHCl is followed by fluorescence spectroscopy. Dependence on t_i of the refolding amplitude corresponding to folding rate constant λ_1 (7.44 s^{-1}) (A), folding rate constant λ_2 (1.21 s^{-1}) (B), and folding rate constant λ_3 (0.30 s^{-1}) (C). A single exponential equation is fitted to all data, and the corresponding fit is represented by a solid line. The amplitude corresponding to λ_1 builds up with a rate of 10.6 $\pm$ 0.8 s^{-1}; in the case of λ_2 the rate of appearance of the corresponding amplitude is 9.60 $\pm$ 0.06 s^{-1}; in the case of λ_3 the rate of appearance of the corresponding amplitude is 0.137 $\pm$ 0.005 s^{-1}. The final protein concentration is 1 μM in 100 mM potassium pyrophosphate, pH 6.0, at 25 °C.

λ_1 to λ_4) on t_i clarifies whether a specific refolding process originates from the folding mechanism of apoflavodoxin or from secondary processes in the unfolded protein, such as Xaa−Pro peptide bond isomerization. In the former case, the dependence of the amplitude of a specific refolding process on t_i equals the unfolding rate (9 s^{-1}), whereas in the latter case the t_i dependence of the amplitude is much slower (*38*). Due to the large difference between the λ_1 and λ_4 rate constants, it is not possible to resolve all refolding processes in one kinetic trace in the interrupted unfolding experiment. Traces of 5 s are recorded to sample λ_1, λ_2, and λ_3, and the fourth process is examined separately in a manual mixing experiment, as the rate constant λ_4 is sufficiently slow to do so.

In Figure 5 the refolding amplitudes corresponding to the refolding rate constants λ_1, λ_2, and λ_3 obtained in the interrupted unfolding experiment are shown as a function of the unfolding time t_i. Both refolding amplitudes corresponding to λ_1 and λ_2 appear with rate constants that are in good agreement with the apoflavodoxin unfolding rate constant of 9 s^{-1} under these conditions. This shows that the two faster folding processes represent two parallel folding routes accessible to apoflavodoxin molecules with all prolyl peptide bonds in the native trans conformation. In contrast, the refolding amplitude corresponding to rate constant λ_3 appears with a rate of only 0.14 s^{-1}, which is a very likely rate for proline peptide bond isomerization (*38*). The manual interrupted unfolding experiment shows that the λ_4 refolding amplitude appears with a rate of 0.015 s^{-1} (data not shown), which is compatible with proline peptide bond isomerization as well. Thus, only folding rate constants λ_1 and λ_2 inform about the mechanism that describes apoflavodoxin folding, as the corresponding molecules are shown to have all peptide bonds in the native trans conformation.

(d) GuHCl Dependence of the Apoflavodoxin Folding and Unfolding Kinetics. To obtain more insight into the origin of the observed complexity in apoflavodoxin folding, we performed kinetic refolding and unfolding experiments followed by fluorescence spectroscopy at different GuHCl concentrations. Three or four exponentials are required to describe the observed apoflavodoxin refolding kinetics up to 2 M GuHCl. In contrast, apoflavodoxin unfolding traces are in most cases described by a single exponential. Only in the transition zone of denaturation, where both folding and unfolding processes significantly contribute to the observable rates, are the slower folding processes observed in kinetic unfolding traces. The fastest step observed in kinetic folding is not observed in the kinetic unfolding traces. The four observed rate constants for apoflavodoxin folding and unfolding are shown in Figure 6A as a chevron plot. Figure 6B shows that the complete difference in fluorescence intensity between native and unfolded apoflavodoxin is observed at all concentrations of denaturant used in the kinetic experiments. This means that all processes with a significant corresponding change in fluorescence are observed in the stopped-flow experiments.

(e) Involvement of an On-Pathway Intermediate during Apoflavodoxin Unfolding. Under strong denaturing conditions (>2.5 M GuHCl), a single unfolding rate constant is observed, which displays a smooth curvature as a function of the GuHCl concentration (Figure 6A). This curvature is explained by the presence of two consecutive transition states on one linear apoflavodoxin (un)folding route that both have differing dependencies on the denaturant concentration (Figure 6C). At any denaturant concentration the transition state with the highest free energy determines the observed rate of folding and unfolding. Below approximately 4 M GuHCl TS1 has the highest free energy of both transition states involved. TS1 is less structured than TS2. Consequently, an increase of the denaturant concentration stabilizes TS1 more than TS2, and above approximately 4 M GuHCl TS2 becomes the rate-limiting transition state for apoflavodoxin unfolding. This causes the curvature in the unfolding limb of the chevron plot (Figure 6A). Of the two transition states involved, TS2 cannot be the one having the highest free energy below 4 M GuHCl, because if that would be the case increasing the GuHCl concentration above 4 M would not result in the observed change of the rate-limiting unfolding process.

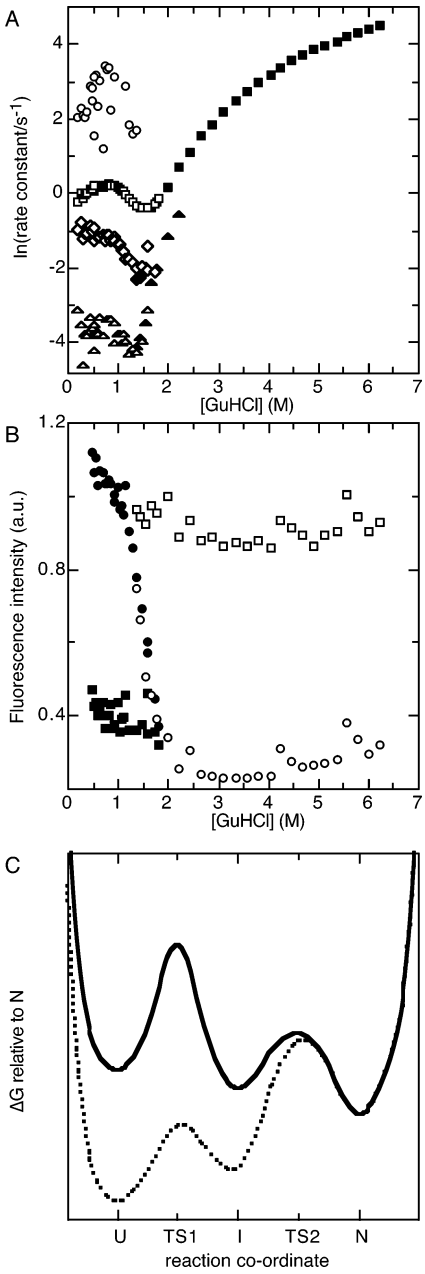

FIGURE 6: (A) GuHCl dependence of the natural logarithm of the observed rate constants (○ = λ_1, □ = λ_2, ◇ = λ_3, △ = λ_4) for *A. vinelandii* apoflavodoxin unfolding (filled symbols) and refolding (open symbols). (B) Initial (□) and final (○) fluorescence intensity of the kinetic traces obtained for apoflavodoxin stopped-flow refolding (filled symbols) and unfolding (open symbols). The final protein concentration is 1 μM in 100 mM potassium pyrophosphate, pH 6.0, at 25 °C. (C) Schematic free energy landscape for the folding of a hypothetical protein via an on-pathway intermediate. The on-pathway intermediate (I) is surrounded by two transition states: TS1 separates I from the unfolded state (U), and TS2 separates I from the native state of the protein (N). At low GuHCl concentrations (solid line) TS1 has the highest free energy of both transition states involved. Above a certain GuHCl concentration (dashed line) TS2 becomes the rate-limiting transition state for unfolding of the protein.

The presence of two transition states, the free energies of which have differing denaturant concentration dependencies, that are each positioned on a separate apoflavodoxin folding route cannot explain the observed curvature in the unfolding limb of λ_2. In this situation, an upward curvature of the unfolding limb would be observed as the unfolding molecules would follow the route with the lowest free energy barrier at all concentrations of denaturant (*11*, *39*). This is clearly not the case (Figure 6A).

Another alternative explanation for the observed curvature in the λ_2 unfolding limb of the apoflavodoxin chevron plot could be a transition state, which separates N from U, that shifts gradually as a function of denaturant concentration. However, this phenomenon has been studied in detail recently and is shown to be highly unlikely (*40*).

Two consecutive transition states on a linear apoflavodoxin (un)folding route that links unfolded and native apoflavodoxin molecules explain the curvature of the λ_2 unfolding limb. A minimum in the free energy between these two transition states must exist. In this minimum an on-pathway folding intermediate resides (Figure 6C). The rate-limiting step during apoflavodoxin unfolding changes between 3 and 5 M GuHCl from the unfolding of this intermediate (i.e., I to U) at low denaturant concentrations to the formation of this intermediate (i.e., N to I) at high denaturant concentrations. Consequently, at intermediate denaturant concentrations (i.e., 2−4 M GuHCl) this intermediate is expected to transiently populate during kinetic apoflavodoxin unfolding. However, only a single unfolding process is observed at all denaturant concentrations above 2.5 M GuHCl (Figure 6A), and the fluorescence intensity does not change during the dead time of the experiment (Figure 6B). Fluorescence anisotropy also shows no additional kinetic phases or dead time processes during kinetic apoflavodoxin unfolding (data not shown). No population of the on-pathway apoflavodoxin folding intermediate is thus observed.

In conclusion, the intermediate that causes the curvature observed in the unfolding limb of the λ_2 chevron plot of apoflavodoxin must be a high-energy on-pathway folding intermediate, as it is not populated to a significant extent. Such high-energy on-pathway intermediates appear to play a role in the folding kinetics of many proteins (*11*, *39*).

(f) Involvement of an Off-Pathway Intermediate during Apoflavodoxin Folding. Under conditions where apoflavodoxin is fully native (<1 M GuHCl), two folding rate constants (i.e., λ_1 and λ_2) are observed that do not originate from Xaa−Pro peptide bond isomerizations. The observation of these two folding rates implies that an intermediate populates significantly during refolding of apoflavodoxin. Is the intermediate that populates during refolding the same species as the one that causes the curvature in the unfolding limb of the chevron plot? If that would be the case, a three-state protein folding model would be able to describe the observed apoflavodoxin λ_2 chevron plot. However, the denaturant dependence of λ_2 cannot be described by any three-state folding mechanism, be it linear with an on-pathway intermediate involved (U ⇔ I ⇔ N) or linear with an off-pathway intermediate involved (I ⇔ U ⇔ N) or triangular with all three species (U, I, N) being connected (results not shown). Thus at least two folding intermediates must play a role during kinetic (un)folding of apoflavodoxin.

Additional evidence that the on-pathway intermediate does not populate significantly during apoflavodoxin refolding comes from the interrupted refolding experiment. In case formation of an on-pathway apoflavodoxin intermediate during folding is more rapid than its conversion to the native state, the intermediate accumulates, and formation of native molecules is delayed (*12*). The kinetic formation of native

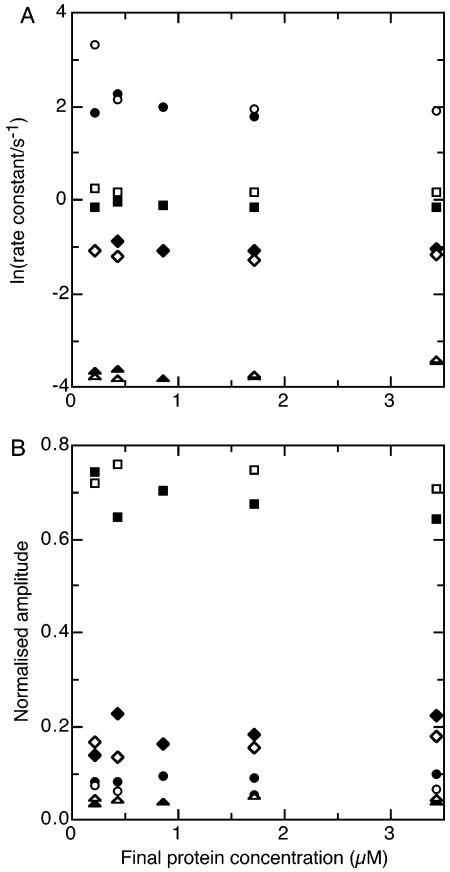

FIGURE 7: Dependence of the natural logarithm of the observed rate constants ($\bigcirc = \lambda_1$, $\square = \lambda_2$, $\diamond = \lambda_3$, $\triangle = \lambda_4$) (A) and of the corresponding amplitudes (B) on protein concentration at 0.27 M GuHCl (filled symbols) and at 0.59 M GuHCl (open symbols) for *A. vinelandii* apoflavodoxin folding. Folding is started from equilibrium unfolded apoflavodoxin in 3.0 M GuHCl. The buffer used is 100 mM potassium pyrophosphate, pH 6.0, at 25 °C.

molecules is then characterized by the presence of a lag phase, which is clearly not observed during the interrupted apoflavodoxin refolding experiment (Figure 4). The on-pathway intermediate is besides being unstable under denaturing conditions (>2.5 M GuHCl) thus also unstable under native conditions. The intermediate that populates during apoflavodoxin refolding must be a different one than the on-pathway intermediate already discussed.

The folding limb of the λ_2 chevron plot curves to such an extent that at low denaturant concentration the observed folding rate actually increases with increasing GuHCl concentration (Figure 6A). The latter is characteristic for an unfolding process. Dissociation of dimers or higher oligomeric states that may be transiently formed during apoflavodoxin refolding can be excluded as a source for the observed curvature, since variation of the final protein concentration from 0.2 to 3.4 μM did not significantly alter the observed rate constants nor their relative amplitudes during refolding (Figure 7).

The curvature of the folding limb of the λ_2 chevron plot is explained by the transient population of a folding intermediate which is off the productive folding route. The unfolding of this off-pathway intermediate is the rate-limiting step in the formation of native apoflavodoxin via the process corresponding to λ_2. In principle, the partial unfolding of an on-pathway intermediate could also be the rate-limiting process during protein folding. However, if such an intermediate transfers to native apoflavodoxin with rate constant λ_2, a delay in the formation of native apoflavodoxin would be observed, which is not the case.

The interrupted refolding experiment confirms that an off-pathway intermediate populates during apoflavodoxin folding. In case an off-pathway intermediate that needs to unfold en route to the native state populates, native protein forms kinetically with a sum of two exponentials. The latter is exactly as is observed in the interrupted refolding experiment, besides the observation of rate constants associated with peptide bond isomerization processes. At low denaturant concentrations (<0.75 M GuHCl) λ_2 represents the kinetic formation of native apoflavodoxin via an off-pathway intermediate, whereas λ_1 at these concentrations reflects the direct kinetic formation of native apoflavodoxin by those molecules that circumvent the off-pathway intermediate. From the interrupted refolding experiment (Table 2) it can be inferred that $10.6 \pm 0.4\%$ and $11 \pm 2\%$ of the molecules with native proline peptide bonds fold via the direct path to the native state at 0.42 and 0.83 M GuHCl, respectively [as determined via $A_1/(A_1 + A_2)$ (Table 2)]. The majority of the apoflavodoxin molecules thus folds via the off-pathway apoflavodoxin folding intermediate.

(g) The Equilibrium Folding Intermediate of Apoflavodoxin Is Not the Kinetic On-Pathway Intermediate. Are the intermediate that populates during equilibrium denaturation of apoflavodoxin and the kinetic on-pathway intermediate the same species? To answer this question, kinetic folding and unfolding experiments that start with apoflavodoxin in 1.6 M GuHCl were done. Under these conditions the *A. vinelandii* apoflavodoxin equilibrium intermediate is near to maximally populated (for 55%; Figure 2E).

In case the apoflavodoxin on-pathway intermediate is the equilibrium intermediate, what folding and unfolding kinetics are expected starting with apoflavodoxin in 1.6 M GuHCl? Below a final GuHCl concentration of approximately 4 M, the rate constant for folding of the on-pathway intermediate to native apoflavodoxin is determined by TS2, and the rate constant for folding from globally unfolded apoflavodoxin to native apoflavodoxin is determined by TS1 (Figure 6C). As under these circumstances TS1 has a higher free energy than TS2, the on-pathway intermediate folds faster to the native state than unfolded apoflavodoxin does. The latter kinetic behavior is clearly not observed when starting with the equilibrium intermediate of apoflavodoxin populated: the observed folding rate constants are identical to the folding rate constants observed in the classical chevron experiment already discussed (Figure 8A). In addition, the total amplitude of the folding reaction is the same in both experiments (Figure 8B), as well as the relative amplitude of each of the four folding processes (Figure 8C).

Above a final GuHCl concentration of approximately 4 M, the rate constant for unfolding of the on-pathway intermediate is determined by TS1, whereas the rate constant for unfolding of native apoflavodoxin is determined by TS2, which at these denaturant concentrations has a higher free energy than TS1 (Figure 6C). Consequently, under these circumstances the on-pathway intermediate needs to unfold faster than native apoflavodoxin does. No such fast unfolding process is observed when the equilibrium folding intermediate is populated (Figure 8A). However, the equilibrium

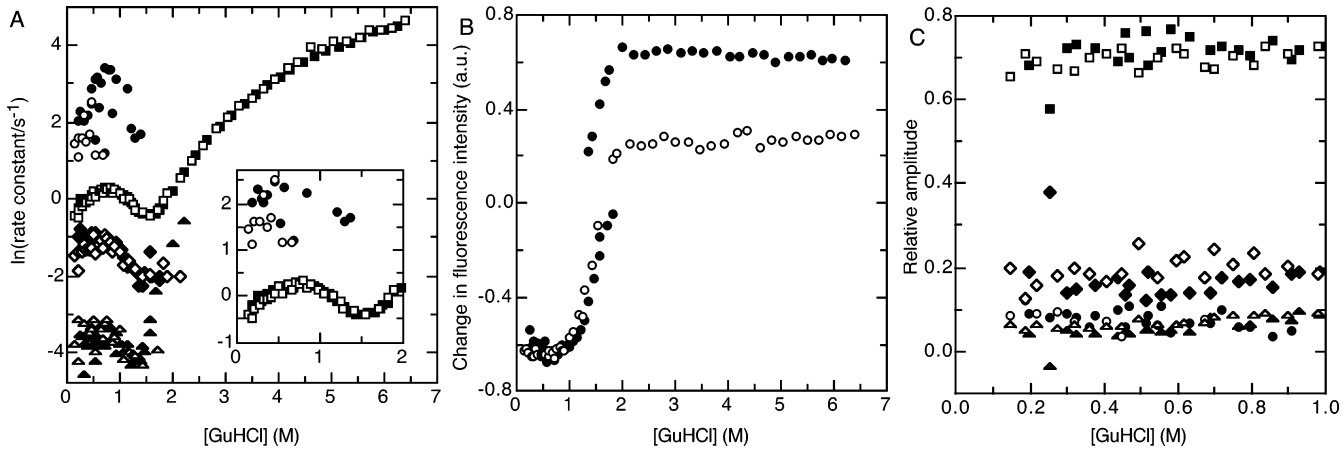

FIGURE 8: (A) GuHCl dependence of the natural logarithm of the observed rate constants (○ = λ_1, □ = λ_2, ◇ = λ_3, △ = λ_4) for *A. vinelandii* apoflavodoxin unfolding and refolding. Open symbols: folding and unfolding are both started with apoflavodoxin in 1.6 M GuHCl, the concentration GuHCl at which 55% of the apoflavodoxin molecules is present as the equilibrium folding intermediate (see Figure 2E). Filled symbols are the data presented in Figure 6; folding is here started with unfolded apoflavodoxin (at 5 M GuHCl), and unfolding is here started with native apoflavodoxin (at 0 M GuHCl). The inset shows a zoom of λ_1 and λ_2 at GuHCl concentrations below 2 M. (B) GuHCl dependence of the total fluorescence intensity change (i.e., the initial minus the final fluorescence intensity) during kinetic apoflavodoxin folding and unfolding starting with apoflavodoxin in 1.6 M GuHCl (○). The GuHCl dependence of the total change in fluorescence intensity during kinetic folding starting with unfolded apoflavodoxin (at 5 M GuHCl) and during kinetic unfolding starting with native apoflavodoxin (at 0 M GuHCl) is also shown (●). (C) GuHCl dependence of the relative amplitudes corresponding to each of the four observed apoflavodoxin folding processes (○ = A_1, □ = A_2, ◇ = A_3, △ = A_4). Open symbols represent amplitudes of folding processes starting with apoflavodoxin in 1.6 M GuHCl, whereas filled symbols represent amplitudes of folding processes starting with unfolded apoflavodoxin in 5 M GuHCl. The final protein concentration is 1 μM in 100 mM potassium pyrophosphate, pH 6.0, at 25 °C.

intermediate still could be the kinetic on-pathway intermediate, but the unfolding of this equilibrium intermediate could be too fast to be detected. In that case, the amplitude associated with this unfolding process should decrease between 3 and 5 M GuHCl (as in this GuHCl concentration range the free energy of TS1 gradually becomes lower than the one of TS2) and then level off horizontally. However, no such change in amplitude is observed as well (Figure 8B). Rather, Figure 8B shows that the amplitude of the unfolding process starting with the equilibrium intermediate populated is constant and drastically reduced compared to the situation in which unfolding starts with native apoflavodoxin. Both below and above 4 M GuHCl, unfolding of the equilibrium intermediate occurs within the dead time of the stopped-flow unfolding experiment and thus is faster than unfolding of native apoflavodoxin.

In conclusion, the experiments described show that the intermediate that is observed during equilibrium denaturation of *A. vinelandii* apoflavodoxin cannot be the on-pathway intermediate observed during kinetic apoflavodoxin folding.

(h) Kinetic Role of the Equilibrium Folding Intermediate of Apoflavodoxin. Is the intermediate observed during equilibrium denaturation of apoflavodoxin the kinetic off-pathway intermediate that populates during apoflavodoxin folding? If this is the case, its unfolding should be observed at all GuHCl concentrations above at which it maximally populates, i.e., above approximately 1.8 M GuHCl (Figure 2E). Indeed, a loss of the amplitude of the unfolding process is observed when unfolding starts with the equilibrium intermediate populated compared to when unfolding starts with native apoflavodoxin (Figure 8B).

Further confirmation of the equilibrium intermediate being the kinetic off-pathway intermediate comes from the following. The spectroscopic properties of the apoflavodoxin equilibrium intermediate are remarkably similar to those of the kinetic off-pathway folding intermediate. The intermediate that populates during equilibrium denaturation of apoflavodoxin has a low fluorescence emission (Figure 2F). The kinetic apoflavodoxin off-pathway intermediate must also have a low fluorescence intensity, as is discussed below. The interrupted refolding experiment shows that approximately 90% [i.e., $A_2/(A_1 + A_2)$%, Table 2] of the folding apoflavodoxin molecules with native Xaa−Pro peptide bonds populate the off-pathway intermediate and form native apoflavodoxin with rate constant λ_2. The direct refolding experiment shows that the amplitude corresponding to λ_2 is also approximately 90% of the total amplitude caused by apoflavodoxin molecules with native Xaa−Pro peptide bonds (as can be inferred from A_1 and A_2 shown in Figure 8C). In this direct refolding experiment, the amplitude of λ_2 corresponds to the change in fluorescence intensity. Consequently, the fluorescence intensity of the off-pathway intermediate must be similar to the fluorescence intensity of unfolded apoflavodoxin, as is also observed for the equilibrium intermediate (Figure 2F). In addition, when kinetic folding of apoflavodoxin is followed by fluorescence anisotropy, large anisotropy is observed immediately after the dead time of the experiment. This anisotropy subsequently decreases with rate constant λ_2 (not shown). As the folding process with rate constant λ_2 represents the unfolding of the off-pathway intermediate, the latter intermediate must have a high anisotropy. As discussed, a high anisotropy signal is also observed for the equilibrium folding intermediate.

In conclusion, the results presented show that the *A. vinelandii* apoflavodoxin equilibrium folding intermediate and the intermediate that appears kinetically off the productive apoflavodoxin folding route most likely are the same species.

(i) Quantitative Kinetic Model for Apoflavodoxin Folding. Based on the apoflavodoxin folding data presented here, a kinetic model for apoflavodoxin folding is constructed, as shown in Scheme 1, with I_1 being the off-pathway kinetic

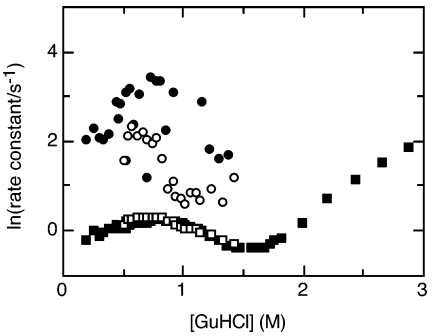

FIGURE 9: GuHCl dependence of the natural logarithm of the observed rate constants for *A. vinelandii* apoflavodoxin folding (○ = λ_1, □ = λ_2) obtained by starting with equilibrium unfolded apoflavodoxin (filled symbols) or by starting with freshly unfolded apoflavodoxin, made by unfolding apoflavodoxin for 622 ms in 3 M GuHCl (open symbols). The final protein concentration is 1 μM in 100 mM potassium pyrophosphate, pH 6.0, at 25 °C.

folding intermediate that is stable and also populates during equilibrium denaturation of apoflavodoxin, I_2 the high-energy on-pathway kinetic folding intermediate, U the unfolded state, and N native apoflavodoxin. Scheme 1 is the most simple model containing two intermediates that is able to explain the observations made on apoflavodoxin folding.

Scheme 1

$$I_1 \underset{k_{UI_1}}{\overset{k_{I_1U}}{\rightleftharpoons}} U \underset{k_{I_2U}}{\overset{k_{UI_2}}{\rightleftharpoons}} I_2 \underset{k_{NI_2}}{\overset{k_{I_2N}}{\rightleftharpoons}} N$$

In the case of any four-state kinetic folding model, three observable rate constants are expected (*28*, *36*, *41*). However, since one of the four apoflavodoxin species is very unstable (i.e., the on-pathway intermediate), only two rate constants that inform about apoflavodoxin folding are observed (i.e., λ_1 and λ_2). The latter is highly homologous to the case of apparent two-state folding, where a single rate constant is observed with a curvature of the unfolding limb of the chevron plot, which is due to the presence of a high-energy on-pathway intermediate, as discussed in detail recently by Sánchez and Kiefhaber (*11*).

Normally, a kinetic protein folding model is fitted to the GuHCl dependence of all observed kinetic folding rates and corresponding amplitudes that are not due to Xaa−Pro isomerizations, i.e., λ_1 and λ_2 in the case of *A. vinelandii* apoflavodoxin folding. However, the fastest process observed during apoflavodoxin folding, with observed rate constant λ_1, displays a lot of scatter (Figure 6), which is mainly due to its small amplitude. The scatter may in part also be caused by contributions of additional processes with similar rates, e.g., the rapid formation of intermediates with non-native peptide bond isomers. To investigate the influence of Xaa−Pro peptide bond isomerization on λ_1, an experiment is performed in which freshly unfolded apoflavodoxin (made by unfolding the protein for 622 ms in 3 M GuHCl) is refolded at different GuHCl concentrations. Refolding of freshly unfolded apoflavodoxin leads to an observed rate constant λ_1 which differs from the one obtained by starting with equilibrium-unfolded apoflavodoxin, as is shown in Figure 9. The observed rate constant λ_2 of the major folding process obtained by refolding freshly unfolded apoflavodoxin is identical within error to λ_2 obtained in the conventional refolding experiment in which equilibrium-unfolded apoflavodoxin is used. The observed change in rate constant λ_1 indeed shows that in the conventional refolding experiment λ_1 is influenced by the formation of intermediates with incorrect proline isomers. Unfortunately, even the refolding process starting from freshly unfolded apoflavodoxin results in a complex GuHCl concentration dependence of the observed rate constant λ_1, which curves downward upon increasing the denaturant concentration. This curvature cannot be reproduced by a linear four-state model and indicates further complexities in the apoflavodoxin folding mechanism that cannot be resolved accurately. As in the case of *A. vinelandii* apoflavodoxin λ_1 cannot be resolved, only one rate constant (i.e., λ_2) is used in our analysis.

Scheme 1 is fitted to the denaturant dependence of folding rate constant λ_2. Folding rate constant λ_2 is the most informative of the four rate constants observed, as it has the largest amplitude, is observed at all denaturant concentrations, involves native proline peptide bond isomers, and thus informs about the apoflavodoxin folding mechanism. It has a minimum around 1.55 M GuHCl and displays a complex denaturant concentration dependence (Figure 6A). The amplitude A_2 corresponding to λ_2 is not used as it makes no sense to fit a folding model to a single amplitude. The validation of Scheme 1 is obtained in the previous sections by the qualitative analysis of the apoflavodoxin direct and interrupted refolding and unfolding data. Similarly, in the case of hen egg white lysozyme interrupted refolding experiments have also allowed the determination of a complex kinetic folding mechanism without the use of the corresponding kinetic amplitudes (*12*−*14*).

Because only the GuHCl dependence of λ_2 can be analyzed, additional information is required (*28*) to determine unambiguously all microscopic rates shown in Scheme 1. As discussed, the apoflavodoxin equilibrium folding intermediate and the intermediate that appears kinetically off the productive folding route of apoflavodoxin most likely are the same species. We therefore restrained the fit of Scheme 1 to the kinetic apoflavodoxin (un)folding data by fixing K_{UI_1} and m_{UI_1} to the values for K_{UI} and m_{UI} obtained from the equilibrium denaturation measurements (Table 1), according to the equations:

$$\Delta G_{UI_1} = -RT \ln K_{UI_1} = -RT \ln(k_{UI_1}/k_{I_1U}) \qquad (8)$$

$$m_{UI}^{eq} = m_{UI_1} - m_{I_1U} \qquad (9)$$

Since I_2 is shown to never populate significantly during apoflavodoxin folding, k_{I_2N} in Scheme 1 must be much larger than ($k_{UI_2} + k_{I_2U}$), and thus the latter will always limit the observed folding rate. Therefore, k_{I_2N} cannot be determined. The kinetic data can only inform about the relative free energies of the two transition states surrounding I_2, i.e., the ratio between k_{I_2N} and k_{I_2U}. For technical reasons, the ratio is not fitted directly, but instead k_{I_2N} is fixed to 10^5 to be sufficiently large not to influence the observable kinetics. With the assumptions described above, the number of degrees of freedom of the model (Scheme 1) is sufficiently reduced to yield nonredundant results when fitted to the λ_2 chevron obtained for kinetic apoflavodoxin folding.

(j) Free Energy Landscape of Apoflavodoxin Folding. The results of the fit of Scheme 1 to λ_2, using the above

Table 3: Parameters Obtained via the Fit of the Analytical Solution to the Linear Four-State Folding Scheme $I_1 \leftrightarrow$ Unfolded $\leftrightarrow I_2 \leftrightarrow$ Native to the Denaturant Dependence of Rate Constant λ_2 of *A. vinelandii* Apoflavodoxin[a]

k_{I_1U}	0.733 ± 0.002	m_{I_1U}	0.576 ± 0.002
K_{UI}	569	m_{UI}^{eq}	-1.83
k_{UI_1}	417 ± 1	m_{UI_1}	-1.256 ± 0.002
k_{UI_2}	$(7.31 \pm 0.07) \times 10^4$	m_{UI_2}	-4.12 ± 0.01
k_{I_2U}/k_{I_2N}	$(4.02 \pm 0.01) \times 10^{-3}$	$m_{I_2U} - m_{I_2N}$	1.064 ± 0.001
k_{NI_2}	3.234 ± 0.007	m_{NI_2}	0.3218 ± 0.0002
ΔG_{UN}	9.17 ± 0.01	m_{UN}^{eq}	-5.508 ± 0.001

[a] K_{UI} is the equilibrium constant of the I−U equilibrium at zero concentration denaturant, m_{UI}^{eq} is the constant which describes the denaturant concentration dependence of K_{UI}, k_{XY} is the intrinsic rate constant for the transition from state X to Y at zero concentration denaturant, m_{XY} is the factor which describes the denaturant concentration dependence of the rate constant k_{XY}, ΔG_{UN} is the difference in free energy between N and U, and m_{UN}^{eq} describes the denaturant concentration dependence of ΔG_{UN}. Rate constants are in s^{-1}, and m-values are in kcal mol^{-1} M^{-1}. The errors are standard deviations. The equilibrium constant K_{UI} and the corresponding m-value m_{UI}^{eq} are fixed during the fit to the values derived from Table 1. Rate constant k_{UI_1} and m_{UI_1} are calculated using the equilibrium constant K_{UI} and the fitted rate k_{I_1U} and their corresponding m-values, respectively. Rate constant k_{I_2N} is fixed to 100000 and its m-value m_{I_2N} to zero (see text). The exact value of the rate constant k_{I_2U} cannot be determined; the data can only inform about the ratio between k_{I_2N} and k_{I_2U} (see text).

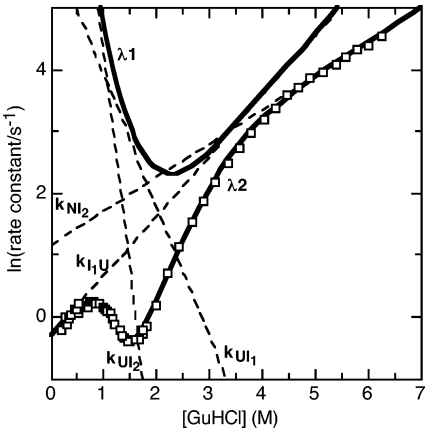

FIGURE 10: Result of the fit of the analytical solution to the linear four-state folding mechanism ($I_1 \leftrightarrow$ unfolded $\leftrightarrow I_2 \leftrightarrow$ native) to the GuHCl dependence of the observed (un)folding rate constant λ_2 (□) of *A. vinelandii* apoflavodoxin as presented in Figure 6. The solid lines represent the fitted denaturant dependence of the observable rate constants λ_1 and λ_2, whereas the dashed lines represent the fitted denaturant dependencies of some of the microscopic rate constants. The numerical results of this fit are summarized in Table 3.

assumptions, are summarized in Table 3 and are shown in Figure 10. The free energy landscape for apoflavodoxin folding derived from the results of the equilibrium and the kinetic folding studies is shown schematically in Figure 11. Note that the on-pathway intermediate I_2 resides in a valley in a region of high free energy at all denaturant concentrations and that the time course of formation of I_2 is always slower than the rate of its further conversion, either to the native or to the unfolded state. As the experimental results show, I_2 never significantly populates, neither kinetically nor at equilibrium, but its presence influences the observed kinetics. Because it never significantly populates, I_2 is classified as a "high-energy" species.

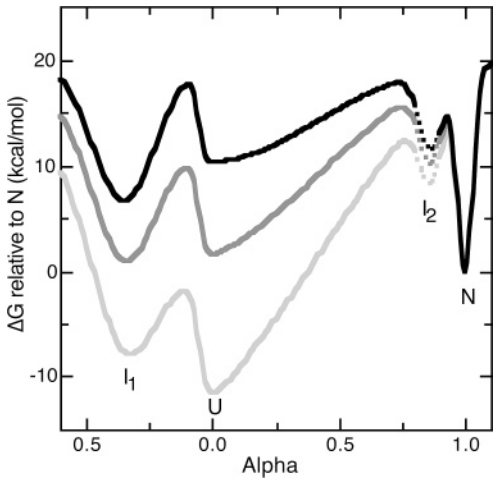

FIGURE 11: Schematic representation of the free energy landscape for *A. vinelandii* apoflavodoxin folding at 0 M (black), 1.6 M (dark gray), and 4 M GuHCl (light gray), derived from the results obtained from equilibrium and kinetic (un)folding studies of the protein. The horizontal axis represents the process coordinate; the vertical axis, the free energy difference relative to native apoflavodoxin. The process coordinate scales to denaturant accessibility, because it is expressed as the α-value, i.e., the ratio of the m-value of a folding species and the m-value of native apoflavodoxin. U and N represent unfolded and native apoflavodoxin, respectively; I_1 and I_2 are the two folding intermediates presented in Scheme 1. The off-pathway intermediate I_1 is represented on the left-hand side of the unfolded state, whereas both the on-pathway intermediate I_2 and native apoflavodoxin reside on the right-hand side of the unfolded state. The heights of the barriers between two species (i and j) were calculated from the (un)folding rates according to $\Delta G_{ij}^{\ddagger} = -RT \ln(k_{ij}/k_0)$ using a value for k_0, the factor describing the chain diffusion rate of a polypeptide, of 10^8 (*47*). The exact position and the depth of the minimum in the free energy landscape in which I_2 resides are unknown and are therefore represented by a dashed line.

Because in the fit of Scheme 1 to the apoflavodoxin folding data the rate constant k_{I_2N} and the corresponding m-value m_{I_2N} are fixed to 100000 s^{-1} and 0 kcal mol^{-1} M^{-1}, respectively, the exact denaturant accessibility of I_2 cannot be calculated. However, the denaturant accessibilities of both transition states surrounding I_2 can be calculated from the kinetic m-values and are expressed as α-values, i.e., the ratio of the m-value of a transition state (TS) and the m-value of the native state, both relative to the unfolded state. The α of TS1 is 0.75, and the α of TS2 is 0.94. Because I_2 must have a solvent accessibility that is between those of the two transition states, it follows that its α is approximately 0.8−0.9.

Besides from equilibrium denaturation experiments, the stability of the native state of apoflavodoxin relative to its unfolded state (ΔG_{UN}) can also be calculated from the kinetically determined folding and unfolding rate constants (Table 3), using an equation analogous to eq 8. The ΔG_{UN} calculated from the kinetic results is 9.17 kcal/mol, which is 1.70 kcal/mol less than the ΔG_{UN} derived from equilibrium denaturation measurements (10.87 ± 0.52 kcal/mol), taking into account the 0.42 kcal/mol due to the Xaa−Pro peptide bond isomerizations. Both ΔG_{UN} values are reasonably similar, and kinetic complexities that cannot be resolved by the current stopped-flow experiments most likely explain the difference in free energy values observed.

In conclusion, a linear four-state folding scheme, $I_1 \leftrightarrow$ unfolded $\leftrightarrow I_2 \leftrightarrow$ native, and its corresponding free energy

landscape are consistent with the experimental data obtained on *A. vinelandii* apoflavodoxin folding.

The Doubly Wound Topology of a Protein Seems To Determine the Appearance of Its Folding Intermediates. The topology of a protein is proposed to control folding. However, little is known about whether topology controls the formation of intermediates and the role they play in the kinetic folding mechanism (*3*, *4*). Comparison of the results obtained here on *A. vinelandii* apoflavodoxin folding with results available on the folding of other $\alpha-\beta$ parallel proteins can shed light onto this issue.

Besides the results presented here on the folding of *A. vinelandii* apoflavodoxin, a rather limited number of kinetic folding experiments have recently been reported for an apoflavodoxin extracted from *Anabaena* (*42*). In the latter study, the initial increase of one of the two observed *Anabaena* apoflavodoxin refolding rates with increasing denaturant concentration suggests that an unfolding step is also rate-limiting for a fraction of the folding *Anabaena* apoflavodoxin molecules. Further details of the kinetic mechanism of *Anabaena* apoflavodoxin folding might be revealed in the future by interrupted refolding and unfolding experiments similar to those presented here for *A. vinelandii* apoflavodoxin.

Another protein that shares the $\alpha-\beta$ parallel topology with apoflavodoxin is CheY (129 amino acids), which is a chemotactic protein, the folding of which has been studied experimentally (*43*). CheY is both sequentially and functionally unrelated to flavodoxins. A structural alignment of 184 backbone atoms of CheY and of *A. vinelandii* apoflavodoxin with an rmsd of 1.62 Å shows 4% sequence identity and 20% similarity according to the PAM250 matrix (*44*). One intermediate has been identified experimentally in CheY folding and is thought to be misfolded, based on the influence of mutations on the folding kinetics (*43*). Inspection of Figure 1D in Lopez-Hernandez et al. (*43*) clearly shows that the kinetic refolding limb of the chevron plot of the Hel2 mutant of CheY, a mutant in which helix 2 has been stabilized, has a positive slope at low denaturant concentrations. In our opinion, this positive slope proves the involvement of an intermediate that is off-pathway. Apparently, an off-pathway intermediate plays an important role in the kinetic folding of all three $\alpha-\beta$ parallel proteins studied to date.

The folding of CheY is also studied theoretically using a simple model for protein folding (*22*), consisting of a Gõ-like potential in which the only forces used arise from contacts that are present in the native state, whereas the energetic frustration is drastically reduced by not including residue-specific parameters. These simulations predict two possible intermediates: a short-lived on-pathway intermediate and an intermediate which is a misfolded trap (*22*). During the simulation, this misfolded species has to unfold, at least partially, before the native state is reached. Since the constraints in the theoretical model of Clementi et al. (*22*) are derived from contacts in the native state of CheY, the results are thought to be universal for proteins that share the doubly wound topology. The kinetic results presented by us on *A. vinelandii* apoflavodoxin lead to the first experimental identification of both intermediates predicted theoretically to occur during the folding of an $\alpha-\beta$ parallel protein.

CONCLUSION

The experimental data obtained on *A. vinelandii* apoflavodoxin folding show that two folding intermediates play a role. The large majority of the folding apoflavodoxin molecules form an intermediate that needs to unfold before becoming productive. All folding apoflavodoxin molecules pass through a second high-energy folding intermediate before reaching the native state. The appearance of both kinetic folding intermediates seems to be governed by protein topology.

ACKNOWLEDGMENT

We are grateful to Andreas Möglich for assistance with MatLab.

REFERENCES

1. Plaxco, K. W., Simons, K. T., and Baker, D. (1998) Contact order, transition state placement and the refolding rates of single domain proteins, *J. Mol. Biol. 277*, 985−994.
2. Grantcharova, V., Alm, E. J., Baker, D., and Horwich, A. L. (2001) Mechanisms of protein folding, *Curr. Opin. Struct. Biol. 11*, 70−82.
3. Clarke, J., Cota, E., Fowler, S. B., and Hamill, S. J. (1999) Folding studies of immunoglobulin-like beta-sandwich proteins suggest that they share a common folding pathway, *Struct. Folding Des. 7*, 1145−1153.
4. Gunasekaran, K., Eyles, S. J., Hagler, A. T., and Gierasch, L. M. (2001) Keeping it in the family: folding studies of related proteins, *Curr. Opin. Struct. Biol. 11*, 83−93.
5. Tanford, C., Aune, K. C., and Ikai, A. (1973) Kinetics of unfolding and refolding of proteins. 3. Results for lysozyme, *J. Mol. Biol. 73*, 185−197.
6. Kuwajima, K., Yamaya, H., Miwa, S., Sugai, S., and Nagamura, T. (1987) Rapid formation of secondary structure framework in protein folding studied by stopped-flow circular dichroism, *FEBS Lett. 221*, 115−118.
7. Matouschek, A., Kellis, J. T., Jr., Serrano, L., Bycroft, M., and Fersht, A. R. (1990) Transient folding intermediates characterized by protein engineering, *Nature 346*, 440−445.
8. Jennings, P. A., and Wright, P. E. (1993) Formation of a molten globule intermediate early in the kinetic folding pathway of apomyoglobin, *Science 262*, 892−896.
9. Baldwin, R. L. (1996) On-pathway versus off-pathway folding intermediates, *Folding Des. 1*, R1−R8.
10. Roder, H., and Colon, W. (1997) Kinetic role of early intermediates in protein folding, *Curr. Opin. Struct. Biol. 7*, 15−28.
11. Sanchez, I. E., and Kiefhaber, T. (2003) Evidence for sequential barriers and obligatory intermediates in apparent two-state protein folding, *J. Mol. Biol. 325*, 367−376.
12. Kiefhaber, T. (1995) Kinetic traps in lysozyme folding, *Proc. Natl. Acad. Sci. U.S.A. 92*, 9029−33.
13. Wildegger, G., and Kiefhaber, T. (1997) Three-state model for lysozyme folding: triangular folding mechanism with an energetically trapped intermediate, *J. Mol. Biol. 270*, 294−304.
14. Bieri, O., Wildegger, G., Bachmann, A., Wagner, C., and Kiefhaber, T. (1999) A salt-induced kinetic intermediate is on a new parallel pathway of lysozyme folding, *Biochemistry 38*, 12460−12470.
15. van Mierlo, C. P., van Dongen, W. M., Vergeldt, F., van Berkel, W. J., and Steensma, E. (1998) The equilibrium unfolding of *Azotobacter vinelandii* apoflavodoxin II occurs via a relatively stable folding intermediate, *Protein Sci. 7*, 2331−2344.
16. van Mierlo, C. P., van den Oever, J. M., and Steensma, E. (2000) Apoflavodoxin (un)folding followed at the residue level by NMR, *Protein Sci. 9*, 145−157.
17. Mayhew, S. G., and Tollin, G. (1992) General properties of flavodoxins, in *Chemistry and biochemistry of flavoenzymes* (Müller, F., Ed.) pp 389−426, CRC Press, Boca Raton, FL.
18. Steensma, E., Nijman, M. J., Bollen, Y. J., de Jager, P. A., van den Berg, W. A., van Dongen, W. M., and van Mierlo, C. P. (1998) Apparent local stability of the secondary structure of *Azotobacter vinelandii* holoflavodoxin II as probed by hydrogen

exchange: implications for redox potential regulation and flavodoxin folding, *Protein Sci. 7*, 306−317.
19. Steensma, E., and van Mierlo, C. P. (1998) Structural characterisation of apoflavodoxin shows that the location of the stable nucleus differs among proteins with a flavodoxin-like topology, *J. Mol. Biol. 282*, 653−666.
20. Gerstein, M. (1997) A structural census of genomes: comparing bacterial, eukaryotic, and archaeal genomes in terms of protein structure, *J. Mol. Biol. 274*, 562−576.
21. Brenner, S. E., Chothia, C., and Hubbard, T. J. (1997) Population statistics of protein structures: lessons from structural classifications, *Curr. Opin. Struct. Biol. 7*, 369−376.
22. Clementi, C., Nymeyer, H., and Onuchic, J. N. (2000) Topological and energetic factors: what determines the structural details of the transition state ensemble and "en-route" intermediates for protein folding? An investigation for small globular proteins, *J. Mol. Biol. 298*, 937−953.
23. Steensma, E., Heering, H. A., Hagen, W. R., and Van Mierlo, C. P. (1996) Redox properties of wild-type, Cys69Ala, and Cys69Ser *Azotobacter vinelandii* flavodoxin II as measured by cyclic voltammetry and EPR spectroscopy, *Eur. J. Biochem. 235*, 167−172.
24. Edmondson, D. E., and Tollin, G. (1971) Chemical and physical characterization of the Shethna flavoprotein and apoprotein and kinetics and thermodynamics of flavin analogue binding to the apoprotein, *Biochemistry 10*, 124−32.
25. Engel, M. F., van Mierlo, C. P., and Visser, A. J. (2002) Kinetic and structural characterisation of adsorption induced unfolding of bovine {alpha}-lactalbumin, *J. Biol. Chem. 8*, 8.
26. Canet, D., Doering, K., Dobson, C. M., and Dupont, Y. (2001) High-sensitivity fluorescence anisotropy detection of protein-folding events: application to alpha-lactalbumin, *Biophys. J. 80*, 1996−2003.
27. Eftink, M. R. (1994) The use of fluorescence methods to monitor unfolding transitions in proteins, *Biophys. J. 66*, 482−501.
28. Ikai, A., and Tanford, C. (1973) Kinetics of unfolding and refolding of proteins. I. Mathematical analysis, *J. Mol. Biol. 73*, 145−163.
29. Schmid, F. X. (1992) Kinetics of unfolding and refolding of single-domain proteins, in *Protein folding* (Creighton, T. E., Ed.) pp 197−241, W. H. Freeman, New York.
30. Otto, M. R., Lillo, M. P., and Beechem, J. M. (1994) Resolution of multiphasic reactions by the combination of fluorescence total-intensity and anisotropy stopped-flow kinetic experiments, *Biophys. J. 67*, 2511−2521.
31. Beechem, J. M., Sherman, M. A., and Mas, M. T. (1995) Sequential domain unfolding in phosphoglycerate kinase: fluorescence intensity and anisotropy stopped-flow kinetics of several tryptophan mutants, *Biochemistry 34*, 13943−13948.
32. Myers, J. K., Pace, C. N., and Scholtz, J. M. (1995) Denaturant *m* values and heat capacity changes: relation to changes in accessible surface areas of protein unfolding, *Protein Sci. 4*, 2138−2148.
33. Rouviere, N., Vincent, M., Craescu, C. T., and Gallay, J. (1997) Immunosuppressor binding to the immunophilin FKBP59 affects the local structural dynamics of a surface beta-strand: time-resolved fluorescence study, *Biochemistry 36*, 7339−7352.
34. Lakowicz, J. R. (1999) *Principles of fluorescence spectroscopy*, 2nd ed., pp 456 and 459, Kluwer Academic/Plenum Publishers, New York.
35. Ptitsyn, O. B. (1992) The molten globule state, in *Protein folding* (Creighton, T. E., Ed.) pp 243−300, W. H. Freeman, New York.
36. Hagerman, P. J., and Baldwin, R. L. (1976) A quantitative treatment of the kinetics of the folding transition of ribonuclease A, *Biochemistry 15*, 1462−1473.
37. Pappenberger, G., Aygun, H., Engels, J. W., Reimer, U., Fischer, G., and Kiefhaber, T. (2001) Nonprolyl cis peptide bonds in unfolded proteins cause complex folding kinetics, *Nat. Struct. Biol. 8*, 452−458.
38. Reimer, U., Scherer, G., Drewello, M., Kruber, S., Schutkowski, M., and Fischer, G. (1998) Side-chain effects on peptidyl-prolyl cis/trans isomerisation, *J. Mol. Biol. 279*, 449−460.
39. Bachmann, A., and Kiefhaber, T. (2001) Apparent two-state tendamistat folding is a sequential process along a defined route, *J. Mol. Biol. 306*, 375−386.
40. Sanchez, I. E., and Kiefhaber, T. (2003) Hammond behavior versus ground-state effects in protein folding: evidence for narrow free energy barriers and residual structure in unfolded states, *J. Mol. Biol. 327*, 867−884.
41. Szabo, Z. G. (1969) Kinetic characterization of complex reaction systems, in *Comprehensive chemical kinetics* (Bamford, C. H., and Tipper, C. F. H., Eds.) pp 1−80, Elsevier, Amsterdam.
42. Fernandez-Recio, J., Genzor, C. G., and Sancho, J. (2001) Apoflavodoxin folding mechanism: An alpha/beta protein with an essentially off-pathway intermediate, *Biochemistry 40*, 15234−15245.
43. Lopez-Hernandez, E., Cronet, P., Serrano, L., and Munoz, V. (1997) Folding kinetics of Che Y mutants with enhanced native alpha-helix propensities, *J. Mol. Biol. 266*, 610−620.
44. Pearson, W. R. (1990) Rapid and sensitive sequence comparison with FASTP and FASTA, *Methods Enzymol. 183*, 63−98.
45. Kraulis, P. J. (1991) MOLSCRIPT: A program to produce both detailed and schematic plots of protein structures, *J. Appl. Crystallogr. 24*, 946−950.
46. Thorneley, R. N. F., Ashby, G. A., Drummond, M. H., Eady, R. R., Hughes, D. L., Ford, G., Harrison, P. M., Shaw, A., Robson, R. L., Kazlauskaite, J., and Hill, H. A. O. (1994) Flavodoxin and nitrogen fixation: Structure, electrochemistry and posttranslational modification by coenzyme A, in *Flavins and flavoproteins 1993* (Yagi, K., Ed.) pp 343−354, Walter de Gruyter, Berlin.
47. Krieger, F., Fierz, B., Bieri, O., Drewello, M., and Kiefhaber, T. (2003) Dynamics of unfolded polypeptide chains as model for the earliest steps in protein folding, *J. Mol. Biol. 332*, 265−274.

BI049545M